Available online at www.sciencedirect.com
SCIENCE DIRECT®
Polymer 45 (2004) 3321–3328
polymer
www.elsevier.com/locate/polymer

The effect of flexible chain length on thermal and mechanical properties of poly(*m*-methylene 2,6-naphthalate)s

Young Gyu Jeong[a], Won Ho Jo[a,*], Sang Cheol Lee[b]

[a]*Hyperstructured Organic Materials Research Center and School of Materials Science and Engineering, Seoul National University, Sun 56-1, Shinlim-Dong, Kwanak-ku, Seoul 151-742, South Korea*

[b]*School of Advanced Materials and Systems Engineering, Kumoh National University of Technology, Kumi 730-701, South Korea*

Received 28 October 2003; received in revised form 5 February 2004; accepted 2 March 2004

Abstract

The effect of flexible chain length on the thermal and mechanical properties such as melting temperature, glass transition temperature, dynamic mechanical relaxation behavior, and uniaxial tensile deformation for melt-quenched poly(*m*-methylene 2,6-naphthalate) (P*m*N) films was investigated using differential scanning calorimeter (DSC), dynamic mechanical thermal analyzer, and universal tensile machine. It was found from DSC thermograms that P*m*Ns with even number of methylene group have higher melting temperatures and faster crystallization rates than P*m*Ns with odd number of methylene group, showing an odd–even fluctuation. The plots of tan δ versus temperature show that all P*m*N samples have three relaxation processes (β, β^*, and α) regardless of the number of methylene group in their backbone. It was found that both β^*- and α-relaxations are cooperative processes and that the activation energies of both relaxations as well as the glass transition temperature associated with the α-relaxation show odd–even fluctuations as a function of the number of methylene group. The initial tensile modulus at the low drawing rate of 0.15 cm/min also shows an odd–even fluctuation. In summary, the macroscopic thermal and mechanical properties of P*m*N such as melting temperature, glass transition temperature, crystallization rate, activation energies of α- and β^*-relaxations, and initial modulus measured under a slow drawing rate exhibit odd–even fluctuations as the number of methylene group in P*m*N increases.

Keywords: Poly(*m*-methylene 2,6-naphthalate); Odd–even fluctuation; Physical properties

1. Introduction

The members belonging to poly(*m*-methylene 2,6-naphthalate) (P*m*N, where *m* denotes the number of methylene group) are semicrystalline polymers whose preparation was first reported in 1969 [1]. The chemical structure of P*m*N is equivalent to that of poly(*m*-methylene terephthalate) (P*m*T) except that a naphthalene ring replaces a benzene ring in P*m*T, as shown in Fig. 1. Since 2,6-naphthalenedicarboxylic acid, a monomer of P*m*N, has been recently produced in large scale, the P*m*N family has been recognized to have high potential as commercial engineering thermoplastics.

Poly(ethylene 2,6-naphthalate) (PEN, $m = 2$) is the most well known polymer among the P*m*N family, since it has superior properties such as chemical resistance, flame resistance, gas barrier property, and high mechanical strength. Its glass transition temperature, melting temperature, and mechanical properties such as tensile modulus and creep resistance are higher than those of poly(ethylene terephthalate) (PET), since the naphthalene ring imparts greater rigidity to the polymer backbone than the benzene ring does in PET. Therefore, numerous studies have been undertaken to investigate the crystalline structure [2–4], morphology [5–8], crystallization and melting behavior [9–15], and mechanical properties [16–22] of PEN. Poly(butylene 2,6-naphthalate) (PBN, $m = 4$) has also several interesting and useful properties as an engineering plastic, viz. thermostability, hydrolytic stability, and gas barrier property. However, there are only a few studies on its crystal structure [23,24], crystallization and melting behavior [25–28]. While polymerization kinetics, rheological, and thermal properties of poly(trimethylene

* Corresponding author. Tel.: +82-2-880-7192; fax: +82-2-885-1748.
E-mail address: whjpoly@plaza.snu.ac.kr (W.H. Jo).

0032-3861/$ - see front matter © 2004 Elsevier Ltd. All rights reserved.
doi:10.1016/j.polymer.2004.03.016

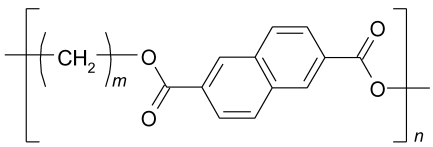

Fig. 1. Chemical structure of poly(*m*-methylene 2,6-naphthalate) (P*m*N).

2,6-naphthalate) (PTN, $m = 3$) have recently been studied [29–33], the crystal structure, crystallization kinetics, melting behavior, and mechanical properties of PTN have not been studied thoroughly. For poly(pentamethylene 2,6-naphthalate) (PPN, $m = 5$), poly(hexamethylene 2,6-naphthalate) (PHN, $m = 6$), and other P*m*Ns ($m > 6$), their crystal structures and thermal properties have not been studied until we have recently synthesized P*m*Ns with the alkylene length of $m = 2$–6 and investigated their crystal structures and thermal properties [34–37]. We have found that PTN and PPN backbone takes *gauche–gauche* conformation in the middle part of each trimethylene and pentamethylene group in their unit cell unlike the crystal structures of PEN, PBN and PHN [35,36]. This indicates that the successive naphthaloyl groups of PTN and PPN are inclined to the crystal *c*-axis by opposite direction, resulting in a Z-shaped arrangement in their respective unit cell. Therefore, it is realized that chain conformation and packing in their unit cell of P*m*Ns with odd number of methylene group differs from that of P*m*Ns with even number of methylene group. Consequently, it is expected that there are some systematic relations between their microscopic chain structure and macroscopic properties such as melting temperature, crystallization rate, and mechanical properties.

In this study, the effect of flexible chain length (m) in P*m*N on their thermal and mechanical properties such as melting temperature, glass transition temperature, dynamic mechanical relaxation behavior, and uniaxial tensile property is systematically investigated using differential scanning calorimeter (DSC), dynamic mechanical thermal analyzer (DMTA), and universal tensile machine.

2. Experimental

All P*m*N samples ($m = 2$–6) used in this study were synthesized by melt–condensation polymerization using tetraisopropyl orthotitanate as a catalyst. In synthesis of P*m*N samples, ethylene glycol ($m = 2$), 1,3-propanediol ($m = 3$), 1,4-butanediol ($m = 4$), 1,5-pentanediol ($m = 5$), and 1,6-hexanediol ($m = 6$) were used as diols, and 2,6-dimethyl naphthalate was used as a dimethyl acetate. The two-stage reaction was performed on a laboratory-scale polymerization reactor. The first-step reaction was the transesterification of 2,6-dimethyl naphthalate with diols under nitrogen atmosphere, and the degree of transesterification was monitored by the amount of methanol distilled as a by-product. The second-step was the polycondensation reaction under high vacuum condition. At the end of reaction, the product in the melt state was quenched into cooling water and then dried in a vacuum oven for several days. The P*m*N samples synthesized in this study were used without any purification. The intrinsic viscosities of all the samples were measured in a mixed solvent of phenol/1,1,2,2-tetrachloroethane (6/4, v/v) using an Ubbelohde viscometer at 35 °C. The intrinsic viscosities of PEN, PTN, PBN, PPN, and PHN were 0.74, 0.74, 0.69, 0.63, and 0.71 dl/g, respectively. This indicates that all the samples synthesized in this study have high molecular weight enough to be formed in film and that the difference of intrinsic viscosities between P*m*N samples is small. Therefore, it is valid to assume that the effect of viscosity difference on thermal and mechanical properties of P*m*N samples is negligibly small.

In order to investigate thermal and mechanical properties of P*m*N, melt-quenched films with 0.2 mm in thickness were prepared by heating the films to the temperature 30 °C higher than their respective melting temperature, holding for 3 min to melt crystals completely, and rapidly transferring into cooling water. Then, the films were dried in a vacuum oven for a day.

Thermal properties of melt-quenched samples were measured with a Perkin–Elmer DSC-7 DSC equipped with an intercooler at the heating rate of 20 °C/min. All DSC runs were carried out under nitrogen atmosphere to minimize oxidative degradation. Before DSC experiment, the baseline was calibrated using an empty crimped aluminum pan, and the melting temperature and the heat of fusion was calibrated using a high-purity indium standard.

The dynamic mechanical experiments of melt-quenched films were performed using a DMTA Mk III instrument in the tensile mode. The dimension of the sample for DMTA was $10.0 \times 5.0 \times 0.2$ mm^3. A peak-to-peak strain of 0.16% was applied at various frequencies of 0.3, 1.0, 3.0, 10.0, and 30.0 Hz. The specimens were run at the heating rate of 0.5 °C/min from -100 °C to above glass transition temperature of the respective sample.

The uniaxial tensile test of melt-quenched samples was carried out using a universal tensile machine (LR 10K, Lloyd Inc.) at three different drawing rates of 0.15, 1.50, and 15.0 cm/min at 25 ± 1 °C. The dimension of sample for uniaxial tensile testing was 50.0 mm long, 5.0 mm wide, and 0.2 mm thick. Nominal stress was calculated from the measured load and the original cross-sectional area of sample. An apparent strain was calculated by dividing the instantaneous displacement (ΔL) in the gauge section by the original gauge length (L_o). Stress–strain curve was obtained by plotting the nominal stress against apparent strain.

To correlate the dynamic mechanical relaxation behavior of P*m*N samples with their uniaxial tensile behavior, it is necessary to find a relationship between the frequency of dynamic mechanical measurement and the drawing rate of tensile test. Although the overall magnitude of strain and the mode of stress used in each test are very different, it is

reasonable to compare the two strain rates at the beginning of the two types of test where the strains are in the linear viscoelastic range. Hence, it is assumed that the frequencies of 0.1, 1.0, and 10.0 Hz in dynamic mechanical experiments are equivalent to the drawing rates of 0.15, 1.50, and 15.0 cm/min in uniaxial tensile tests, respectively [38].

3. Results and discussion

3.1. Thermal property

DSC heating thermograms of melt-quenched P*m*N samples are shown in Fig. 2, where PEN shows glass transition, cold-crystallization, and melting, while PTN and PPN do not show melting on heating thermogram, indicating that the melt-quenched PEN, PTN, and PPN films are in entirely amorphous state. Particularly, PTN and PPN do not show clear crystallization and melting peaks even at a slow heating rate of 2 °C/min, since the crystallization kinetics of these two polymers are very slow [37]. After melt-crystallized for several hours, PTN and PPN show a clear melting transition, as shown in Fig. 2 (dotted lines). On the other hand, PBN has a weak glass transition temperature and a clear melting temperature without cold-crystallization, indicating that the melt-quenched PBN film is in semicrystalline state. It was reported that PBN exhibits fast nucleation and fast crystal growth from the melt, since its chain mobility is large due to flexibility of butylene group as well as favorable interchain interaction between naphthalene rings. Therefore, PBN cannot be obtained in an amorphous state by simply quenching from the melt [39]. PHN also exhibits weak glass transition and clear melting transition on DSC heating thermogram, indicating that it has also fast crystallization rate. However, closer examination of heating thermogram of PHN reveals cold crystallization just above the glass transition. From the above results, it is summarized that the relative crystallization rates of P*m*Ns with even number of methylene group (PEN, PBN, and PHN) are much faster than those of P*m*Ns with odd number of methylene group (PTN and PPN). This is consistent with the result of melt-crystallization experiment that the overall crystallization rate of P*m*N is in the order of PBN > PHN > PEN ≫ PTN > PPN [37]. When the glass transition and melting temperatures of P*m*N obtained from DSC thermograms are plotted against the number of methylene group, as shown in Fig. 3, the melting temperature of P*m*N exhibits an odd–even effect, while the glass transition temperature decreases with increasing the number of methylene group in P*m*N.

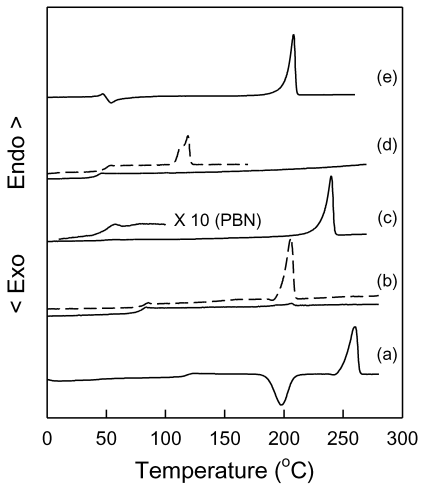

Fig. 2. DSC heating thermograms for P*m*N films: (a) PEN; (b) PTN; (c) PBN; (d) PPN; (e) PHN. The solid lines are for the melt-quenched P*m*N films and the dotted lines for the melt-crystallized PTN and PPN ones.

The X-ray crystallinity (x) for melt-quenched P*m*N films was determined from X-ray diffraction data (Fig. 4) in the range of $2\theta = 5–40°$ using the relation, $x = A_{cr}/(A_{cr} + A_{am})$, where A_{cr} and A_{am} denote the total crystalline and amorphous scattering, respectively, after correction of the Lorentz and polarization factors. The X-ray crystallinity of melt-quenched PBN and PHN films was 5.4 and 3.7%, respectively. The existence of residual crystallinity in the melt-quenched PBN and PHN films may affect their mechanical properties, as will be discussed in Section 3.2.

3.2. Dynamic mechanical thermal analysis

When tan δ measured at various frequencies from 0.3 to 30 Hz is plotted against temperature for melt-quenched P*m*N films, as shown in Fig. 5, it is observed that all the melt-quenched P*m*N films exhibit three relaxation processes (β, β*, and α). Previous investigations on the dynamical properties of PEN have also shown the existence of three relaxation processes [40–47]. Arranged in the order of increasing temperature, these three relaxations are assigned to the local motions of the ester groups (β), the out-of-plane motions of the naphthalene rings or their aggregates (β*), and the long range molecular motions associated with the glass transition (α), respectively. Therefore, it is reasonable

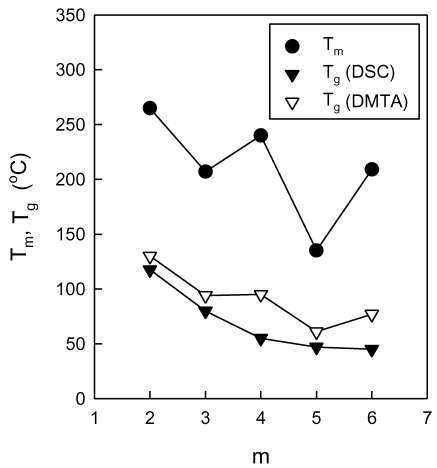

Fig. 3. Melting and glass transition temperatures of P*m*N as a function of the number of methylene group.

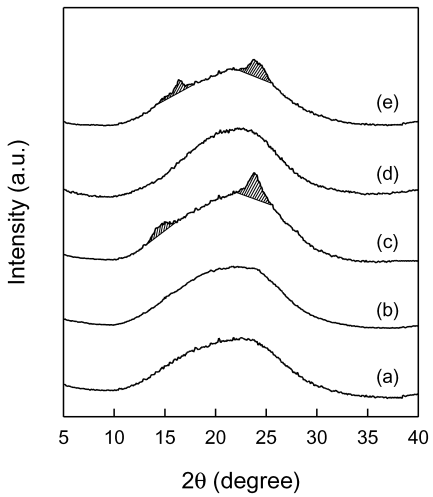

Fig. 4. X-ray diffraction patterns for the melt-quenched P*m*N films: (a) PEN; (b) PTN; (c) PBN; (d) PPN; (e) PHN. The shaded regions in the X-ray patterns of PBN and PHN indicate the scattering from crystalline phase (A_{cr}).

to conclude that all of P*m*N family have similar molecular motions of β-, β*-, and α-relaxation, regardless of the number of methylene group in their backbone. It is also observed from Fig. 5 that α-relaxations for all P*m*N samples is much more intense than β- and β*-relaxations and that the maximum peaks of three relaxation processes (β, β*, and α) shift toward higher temperatures as the frequency increases from 0.3 to 30 Hz. The intensities of β*-relaxations decrease with increasing the frequency, indicating that the molecular motion associated with the β*-relaxation is suppressed as the frequency increases. Another point to be noted from Fig. 5 is that, at a given frequency, the peaks of α-relaxations for PBN and PHN are broader and weaker as compared to those of PEN, PTN, and PPN. This is because the residual crystal in melt-quenched PBN and PHN films reduces the amount of amorphous fraction that contributes to the α-relaxation process. On the other hand, there is an experimental evidence that another portion of the amorphous phase with restricted mobility exists above the glass transition. This phase refers to as the rigid amorphous phase and endows the heterogeneity of the dynamic characteristics of the amorphous fraction in semicrystalline polymers [46]. Therefore, it is realized that the weaker and broader α-relaxation processes of both PBN and PHN films originate from the existence of both residual crystallinity and rigid amorphous phase in melt-quenched samples due to fast crystallization.

When the peak temperature of α-relaxation corresponding to the glass transition temperature is plotted as a function of the number of methylene group, as shown in Fig. 3, two characteristic features are observed. First, the glass transition temperatures obtained from DMTA are higher than the ones obtained from DSC. Second, the glass transition temperatures from DMTA show an odd–even fluctuation depending upon the number of methylene group, whereas the ones from DSC decrease monotonously with increasing the number of methylene group. It is generally accepted that the glass transition temperature from DMTA is 10–15 K higher than the one from DSC. However, unlike PEN, PTN, and PPN, the glass transition temperatures of PBN and PHN obtained from DMTA are about 30 K higher than the ones from DSC. This indicates that the glass transition temperatures obtained from DMTA are more sensitive to the residual crystallinity and rigid amorphous phase than the ones from DSC. Consequently, the glass transition temperatures from DMTA for melt-quenched P*m*N films show an odd–even fluctuation depending on the number of methylene group, as shown in Fig. 3.

Generally, both β- and β*-relaxation processes obey an Arrhenius form, since they are assumed to be thermally activated processes, whereas the α-relaxation process is assumed to follow an empirical Vogel–Fulcher–Tammann (VFT) equation [41,44,46,47]. However, since the plot of the logarithm of frequency versus $1/T$ shows a good linearity in the limited frequency range used in this study, the α-relaxation process can also be described by the Arrhenius equation as follows [42]:

$$f = f_0 \exp[-E_a/RT] \tag{1}$$

where f_0 is a pre-exponential factor, E_a is the activation energy, and R is the gas constant. When the logarithm of frequency is plotted against the reciprocal of peak temperature of tan δ, as shown in Fig. 6, the plots show straight lines and therefore the activation energies of β*- and α-relaxation processes are determined from their slopes. When the activation energy is plotted against the number of methylene group in P*m*N, both β*- and α-relaxation processes exhibit odd–even fluctuations as the number of methylene group increases, as shown in Fig. 7, i.e. P*m*Ns with even number of methylene group has higher activation energy compared to P*m*Ns with odd number of methylene group.

An alternative equation expressing a relationship between frequency and temperature is derived from the Eyring's theory of absolute reaction rate:

$$f = \frac{kT}{2\pi h}\exp[\Delta S/R]\exp[-\Delta H/RT] \tag{2}$$

where ΔS, ΔH, k, and h are the activation entropy, the activation enthalpy, the Boltzmann constant, and the Plank constant, respectively. The activation energy in Eq. (1) is related to the enthalpy in Eq. (2) as follows:

$$E_a = \Delta H + RT - P\Delta V \tag{3}$$

where P is the pressure and ΔV is the activation volume. Neglecting the $P\Delta V$ term due to its small volume change, Eq. (3) combined with Eq. (2) can be expressed as

$$E_a = RT[1 + \ln(kT/2\pi hf)] + T\Delta S \tag{4}$$

For a given temperature and frequency, relaxations are assumed to have a zero activation entropy. This zero

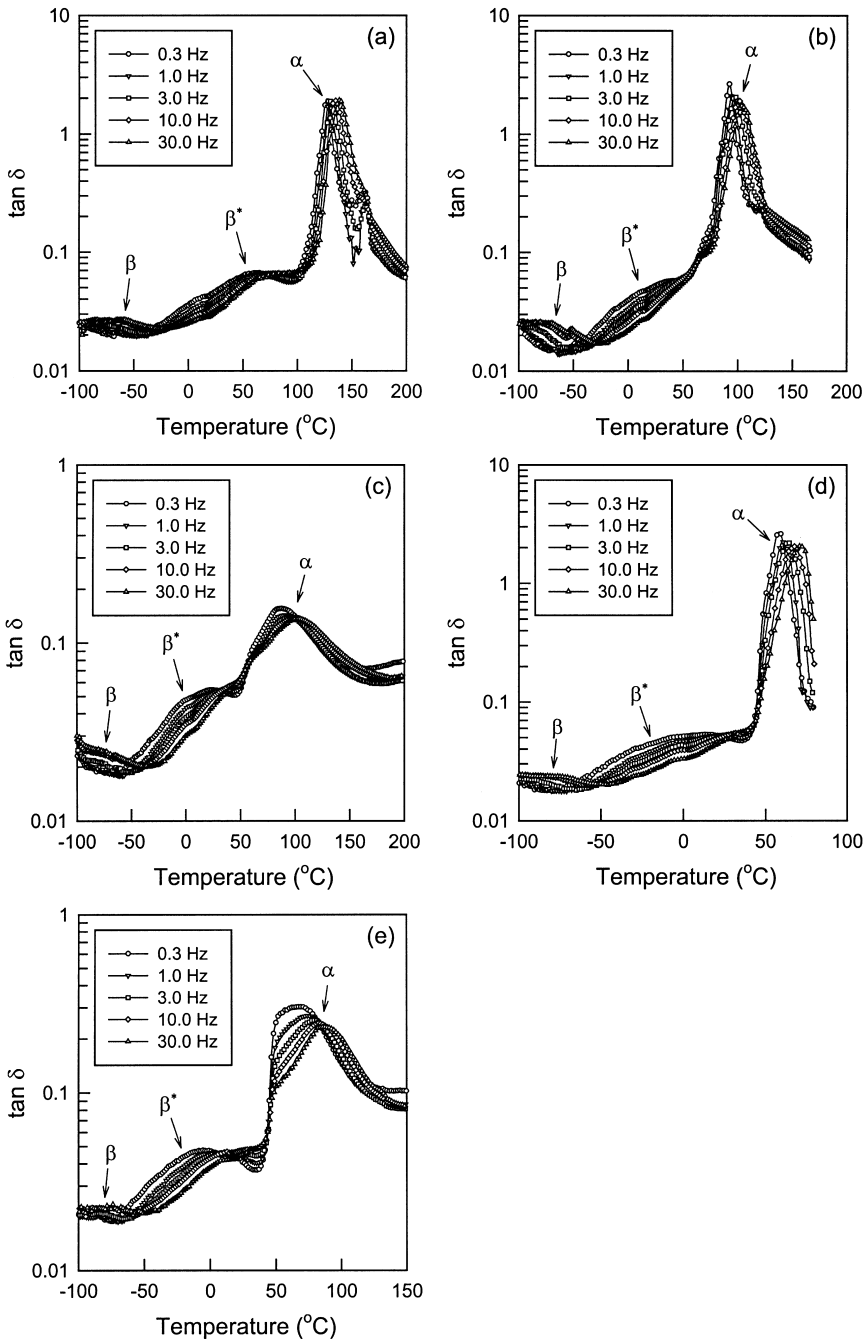

Fig. 5. tan δ versus temperature plots of the melt-quenched P*m*N films at various frequencies: (a) PEN; (b) PTN; (c) PBN; (d) PPN; (e) PHN.

activation entropy corresponds to the lower limit of the activation energy of viscoelastic relaxations. In this case, Eq. (4) with $\Delta S = 0$ reduces to

$$E_a = RT[22.92 + \ln(T/f)] \quad (5)$$

As noted by Starkweather [48–50], this lower limit of the activation energy indicates the relaxation process characterized by local and noncooperative motions (simple relaxations). In such a relaxation process, the interaction between the relaxing molecule and the neighboring one is of short range. On the other hand, the activation energy well above the zero activation entropy condition is ascribed to the relaxation process with cooperative motions (complex relaxations). Therefore, the zero activation entropy criterion can be used as a comparative method that allows to estimate the extent of cooperativity for different relaxation.

A cooperativity plot of the activation energy against relaxation temperature (1 Hz) for DMTA is shown in Fig. 8, where the lower limit of activation energy, i.e. zero activation entropy ($\Delta S = 0$) at 1 Hz, is represented by the solid line. Even though quantitative information such as the extent of cooperativity for molecular motions may not be

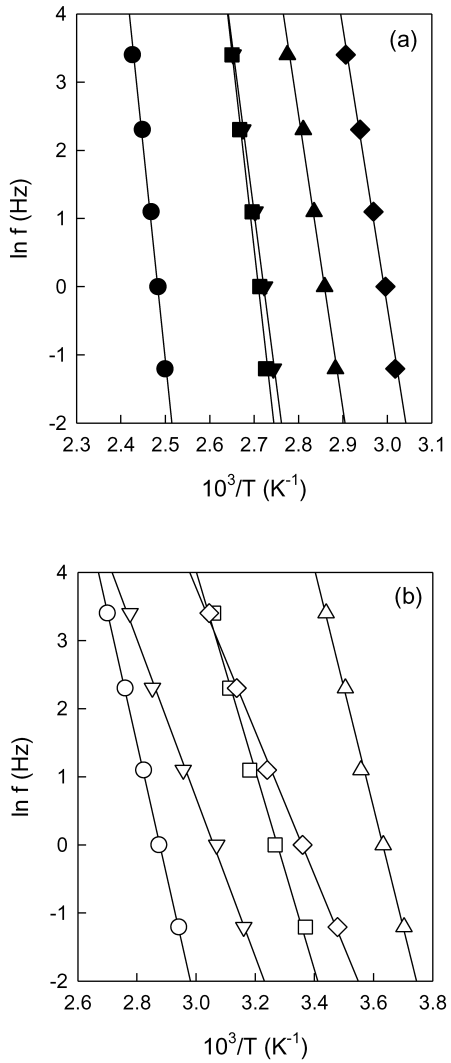

Fig. 6. Dependence of the frequencies of the (a) α- and (b) β*-relaxations with the reciprocal temperatures for PEN (circle), PTN (inverted triangle), PBN (square), PPN (rhombus), and PHN (triangle).

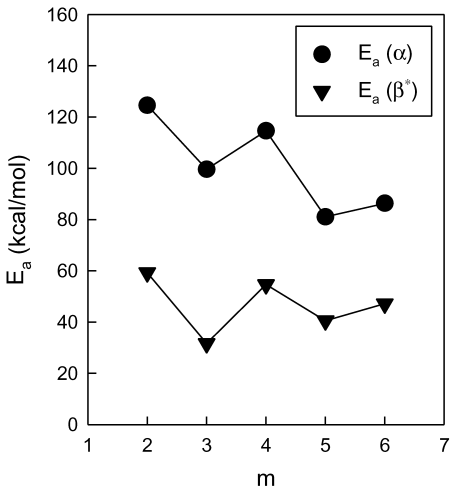

Fig. 7. Activation energies of the α- and β*-relaxation as a function of the number of methylene group.

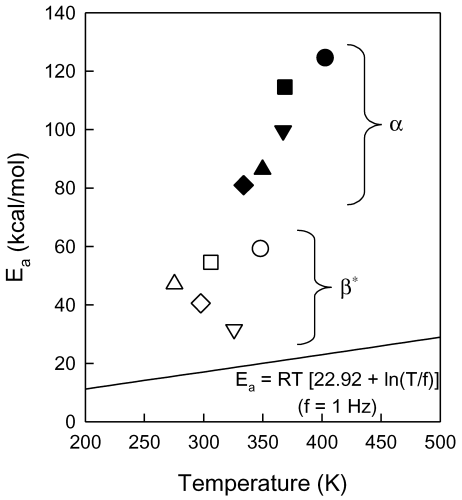

Fig. 8. Cooperative plot for the α- and β*-relaxations of P*m*N: PEN (circle); PTN (inverted triangle); PBN (square); PPN (rhombus); PHN (triangle). The solid line indicates the zero activation entropy criterion at the frequency of 1 Hz.

directly extracted from Fig. 8, it is valid to conclude that both β*- and α-relaxation processes for all P*m*N samples have some cooperativity and that the extent of cooperativity of molecular motions associated with α-relaxation is qualitatively higher than that of β*-relaxation. This result is consistent with the previous studies [46,47] that both β*- and α-relaxation processes of PEN are due to the cooperative molecular motions. It was also reported that the activation energy of β-relaxation for PEN is around 13 kcal/mol [46,47], indicating that the β-relaxation due to local motion of ester groups is noncooperative.

3.3. Uniaxial tensile deformation behavior

The uniaxial tensile tests for melt-quenched P*m*N films were carried out at various drawing rates, and the results were shown in Fig. 9. For all melt-quenched P*m*N samples, the stress–strain curves at the high drawing rate of 15.0 cm/min show immediate rupture without stable necking formation, whereas the curves at the slow drawing rate of 0.15 cm/min exhibit necking and neck propagation. Generally, the tensile deformation behavior of glassy polymers is considered as competition between shear yielding and crazing [38,51,52]. According to the competition, the specimen exhibits either ductile or brittle deformation that is also highly sensitive to the nature of specimen (molecular weight, orientation, crystallinity, defect, etc.), drawing rate, and temperature. At a given condition, the ductile deformation is mainly associated with shear yielding, which is usually followed by necking and neck propagation, whereas the brittle deformation is closely related with crazing which eventually transforms into cracks followed by immediate rupture without forming a stable neck. Therefore, it can be concluded that, for all P*m*N films, the uniaxial tensile behavior at the high drawing rate of

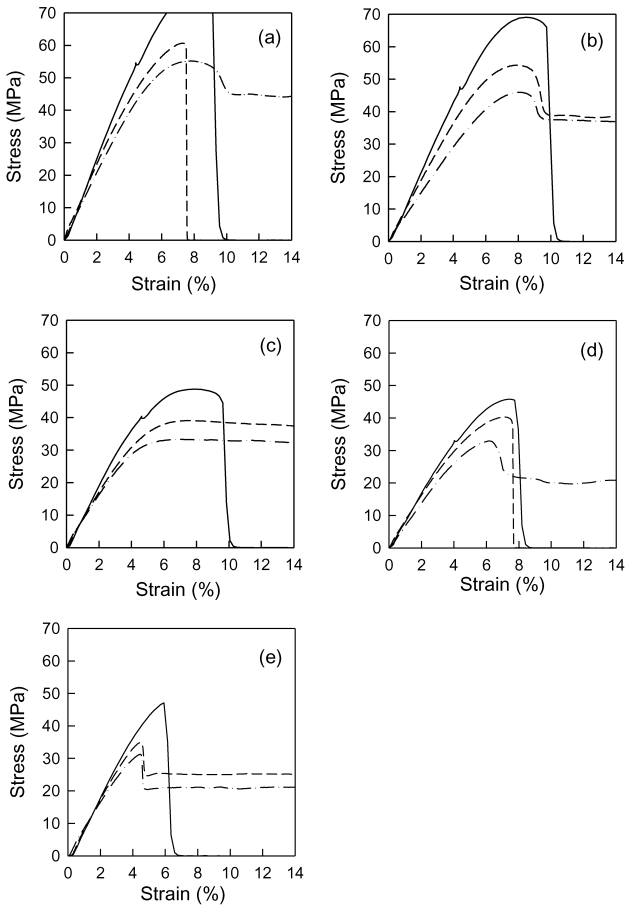

Fig. 9. Stress–strain curves of (a) PEN, (b) PTN, (c) PBN, (d) PPN, and (e) PHN at various drawing rates. The solid, dashed, and dot-dashed lines indicate the drawing rates of 15.0, 1.5, and 0.15 cm/min, respectively.

15.0 cm/min follows brittle deformation, whereas the behavior at the low drawing rate of 0.15 cm/min is ductile deformation. At an intermediate drawing rate of 1.5 cm/min, PTN, PBN, and PHN show ductile deformation, whereas PEN and PPN exhibit brittle deformation.

It has been suggested that the macroscopic mechanical properties are strongly correlated with the secondary relaxation (sub-T_g relaxation) behavior [38,53,54]. It has also been known that the large-scaled main-chain cooperative motion of the secondary relaxation is beneficial for shear yielding. As noted in Section 2, the uniaxial tensile test in this study was carried out around 25 °C which is in the temperature range corresponding to the secondary β*-relaxation for all the melt-quenched P*m*N samples, as can be seen in Fig. 6. Considering the correlation between dynamic frequency and drawing rate and reminding the fact that the intensity of β*-relaxation around room temperature decreases with increasing the frequency from 0.3 to 30 Hz, it is realized that the dependence of tensile deformation on the drawing rate is closely related with the cooperative β*-relaxation process. In short, the brittle tensile deformation behavior at the high drawing rate of 15.0 cm/min is due to suppressed β*-relaxation at room temperature, whereas the ductile deformation behavior at the low drawing rate of 0.15 cm/min is due to enhanced β*-relaxation.

When the initial modulus of P*m*N measured from the stress–strain curve is plotted against the number of methylene group in P*m*N at various drawing rates, as shown in Fig. 10, it reveals that the initial modulus decreases with increasing the number of methylene group and then slightly increases at $m = 6$ at higher drawing rates of 15.0 and 1.5 cm/min. This slight increase of initial modulus at PHN may arise from the fact that the melt-quenched sample of PHN ($m = 6$) shows some degree of crystallinity (3.7%) while the PPN ($m = 5$) sample is in entirely amorphous state. Under the low drawing rate of 0.15 cm/min, however, the initial modulus of P*m*N shows an odd–even fluctuation, which suggests that molecular relaxation of P*m*Ns with odd number of methylene group becomes faster than that of P*m*Ns with even number of methylene group. This is consistent with the dynamic mechanical relaxation behavior showing that the activation energy of P*m*Ns with odd number of methylene group for the cooperative β*-relaxation is lower than that of P*m*Ns with even number of methylene group.

4. Conclusions

The melting temperature and the crystallization rate of P*m*N show an odd–even fluctuation when the property is plotted against the number of methylene group, that is, P*m*Ns with even number of methylene group have higher melting temperatures and faster crystallization rates than P*m*Ns with odd number of methylene group. Plots of tan δ versus temperature measured from dynamic mechanical experiments show that all P*m*N samples have three relaxation processes (β, β*, and α) irrespective of the

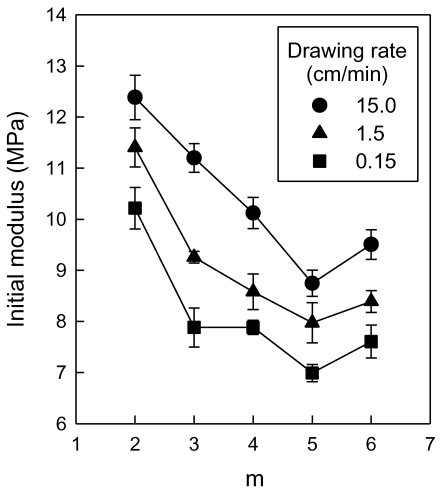

Fig. 10. Initial moduli of the melt-quenched P*m*N films as a function of the number of methylene group when the sample is stretched at various drawing rates.

number of methylene group in their backbone. Arranged in the order of increasing temperature, the three relaxations correspond to the local molecular motions of ester groups (β), the out-of-plane motions of the naphthalene rings or their aggregates (β^*), and the long range molecular motion associated with the glass transition (α), respectively. It was found from dynamic mechanical analysis that the activation energies of both β^*- and α-relaxations as well as the peak temperature of α-relaxation show an odd–even fluctuation as the number of methylene group in P*m*N increases. It was observed from the uniaxial tensile test that the tensile behavior of melt-quenched P*m*N films at the high drawing rate of 15.0 cm/min shows brittle deformation, whereas the tensile behavior at the low drawing rate of 0.15 cm/min exhibits ductile deformation. The ductile or brittle tensile deformation behavior depending on the drawing rate is found to be correlated with the cooperative β^*-relaxation process at room temperature. Therefore, it is concluded that the brittle behavior at the high drawing rate of 15.0 cm/min is due to suppression of β^*-relaxation process, whereas the ductile behavior at the low drawing rate of 0.15 cm/min is due to enhanced β^*-relaxation. The initial modulus at the low drawing rate of 0.15 cm/min shows an odd–even fluctuation as a function of number of methylene group. In summary, the macroscopic properties such as melting temperature, glass transition temperature, crystallization rate, activation energy of α- and β^*-relaxations, and initial modulus of P*m*N show odd–even fluctuations as the number of methylene group in P*m*N increases.

Acknowledgements

The authors thank the Korea Science and Engineering Foundation (KOSEF) for financial support through the Hyperstructured Organic Materials Research Center (HOMRC).

References

[1] Duling IN, Chester W. US Patent 3,436,376; 1969.
[2] Mencik Z. Chem Prum 1976;17(2):78.
[3] Liu J, Sidoti G, Hommema JA, Geil PH, Kim JC, Cakmak M. J Macromol Sci, Phys 1998;B37:567.
[4] Plummer CJG. Macromol Rapid Commun 1999;20:157.
[5] Abis L, Merlo E, Po R. J Polym Sci, Polym Phys Ed 1995;B33:691.
[6] Jakeways R, Klein JL, Ward IM. Polymer 1996;37:3761.
[7] Balta-Calleja FJ, Rueda DR, Michler GH, Naumann I. J Macromol Sci, Phys 1998;B37:411.
[8] Vasanthan N, Salem DR. Macromolecules 1999;32:6319.
[9] Cheng SZD, Wunderlich B. Macromolecules 1988;21:789.
[10] Buchner S, Wiswe D, Zachmann HG. Polymer 1989;30:480.
[11] Kimura FK, Kimura T, Sugisaki A, Komatsu M, Sata H, Ito E. J Polym Sci, Polym Phys Ed 1997;35:2741.
[12] Lee SW, Cakmak M. J Macromol Sci, Phys 1998;B37:501.
[13] Okamoto M, Kubo H, Kotaka T. Macromolecules 1998;31:4223.
[14] Sata H, Kimura T, Ogawa S, Ito E. Polymer 1998;39:6325.
[15] Kajaks J, Flores A, Garcia-Gutierrez MC, Rueda DR, Balta-Calleja FJ. Polymer 2000;41:7769.
[16] Cakmak M, Lee SW. Polymer 1995;36:4039.
[17] Susuki A, Kuwabara T, Kunugi T. Polymer 1998;39:4235.
[18] Susuki A, Nakamura Y, Kunugi T. Polymer 1999;40:5043.
[19] Schoukens G. Polymer 1999;40:5637.
[20] Susuki A, Koide C. J Polym Sci, Polym Phys Ed 2000;38:61.
[21] Karger-Kocsis J, Moskala EJ. Polymer 2000;41:6301.
[22] Arkhireyeva A, Hashemi S. Polymer 2002;43:289.
[23] Watanabe H. Kobunshi Ronbunshu 1976;33:229.
[24] Koyano H, Yamamoto Y, Saito Y, Yamanobe T, Komoto T. Polymer 1998;39:4385.
[25] Chiba T, Asai S, Xu W, Sumita M. J Polym Sci, Polym Phys Ed 1999; 39:561.
[26] Parageorgiou GZ, Karayannidis GP. Polymer 2001;42:2637.
[27] Ju MY, Chang FC. Polymer 2001;42:5037.
[28] Ju MY, Huang JM, Chang FC. Polymer 2002;43:2065.
[29] Tsai RS, Lee YD. J Polym Res 1998;5(2):77.
[30] Hwang SK, Yeh C, Chen LS, Way TF, Tsay LM, Liu KK, Chen LT. Polym Prepr 1999;40:611.
[31] Stier U, Gahr F, Oppermann W. J Appl Polym Sci 2001;80:2039.
[32] Stier U, Oppermann W. J Polym Sci, Polym Phys Ed 2001;39:620.
[33] Stier U, Schawaller D, Oppermann W. Polymer 2001;42:8753.
[34] Jeong YG, Jo WH, Lee SC. Polym J 2001;33:913.
[35] Jeong YG, Jo WH, Lee SC. Polymer 2002;43:7315.
[36] Jeong YG, Jo WH, Lee SC. Polymer 2004;45:379.
[37] Jeong YG. PhD Thesis. Seoul, Korea: Seoul National University; 2003.
[38] Xiao C, Jho JY, Yee AF. Macromolecules 1994;27:2761.
[39] Yamanobe T, Matsuda H, Imai K, Hirata A, Mori S, Komoto T. Polym J 1996;28:177.
[40] Chen D, Zachmann HG. Polymer 1991;32:1612.
[41] Ezquerra TA, Balta-Calleja FJ, Zachmann HG. Acta Polym 1993;44: 18.
[42] Bellomo JP, Lebey T. J Phys D: Appl Phys 1996;29:2052.
[43] Dorlitz H, Zachmann HG. J Macromol Sci, Phys 1997;B36:205.
[44] Canadas JC, Diego JA, Mudarra M, Belana J, Diaz-Calleja R, Sanchis MJ, Jaimes C. Polymer 1999;40:1181.
[45] Canadas JC, Diego JA, Mudarra M, Belana J, Diaz-Calleja R, Sanchis MJ. Polymer 2000;41:2899.
[46] Noglaes A, Denchev Z, Sics I, Ezquerra TA. Macromolecules 2000; 33:9367.
[47] Hardy L, Stevenson I, Boiteux G, Seytre G, Schonhals A. Polymer 2001;42:5679.
[48] Starkweather HW. Macromolecules 1981;14:1277.
[49] Starkweather HW. Macromolecules 1988;21:1798.
[50] Starkweather HW. Polymer 1991;32:2443.
[51] Wellinghoff ST, Baer E. J Appl Polym Sci 1978;22:2025.
[52] Donald AM, Kramer EJ. J Mater Sci 1982;17:1871.
[53] Chen LP, Yee AF, Goetz JM, Schaefer J. Macromolecules 1998;31: 5371.
[54] Chen LP, Yee AF, Moskala EJ. Macromolecules 1999;32:5944.